Production of three-dimensional quantum dot lattice of Ge/Si core-shell quantum dots and Si/Ge layers in an alumina glass matrix

M. Buljan[1*], N. Radić[1], J. Sancho-Paramon [1], V. Janicki[1], J. Grenzer [2], I. Bogdanović-Radović[1], Z. Siketić[1], M. Ivanda[1], A. Utrobičić[3], R. Hübner[2], R. Weidauer[2], V. Valeš[4], J. Endres[4], T. Car[1], M. Jerčinović[1], J. Roško[5], S. Bernstorff[6], V. Holy[4]

[1]Rudjer Bošković Institute, Bijenička cesta 54,10000 Zagreb, Croatia
[2]Helmholtz-Zentrum Dresden-Rossendorf, Germany
[3]University of Zagreb, Zagreb, Croatia
[4]Charles university in Prague, Prague, Czech Republic
[5]Institute of Cell Biology, University of Edinburgh, Mayfield Road, Edinburgh, UK
[6]Elettra-Sincrotrone Trieste, 34149 Basovizza, Italy

E-mail: email:mbuljan@irb.hr

February 2014

Abstract. We report on the formation of Ge/Si quantum dots with core/shell structure that are arranged in a three-dimensional body centered tetragonal quantum dot lattice in an amorphous alumina matrix. The material is prepared by magnetron sputtering deposition of Al_2O_3/Ge/Si multilayer. The inversion of Ge and Si in the deposition sequence results in the formation of thin Si/Ge layers instead of the dots. Both materials show an atomically sharp interface between the Ge and Si parts of the dots and layers. They have an amorphous internal structure that can be crystallized by an annealing treatment. The light absorption properties of these complex materials are significantly different compared to films that form quantum dot lattices of the pure Ge, Si or a solid solution of GeSi. They show a strong narrow absorption peak that characterizes a type II confinement in accordance with theoretical predictions. The prepared materials are promising for application in quantum dot solar cells.

Keywords: Ge/Si core shell, 3D QD lattices, Type II confinement, Absorption Submitted

to: *Nanotechnology*

1. Introduction

Small Ge/Si and Si/Ge quantum dots (QDs) with a core-shell structure are very interesting due to the strong three-dimensional (3D) confinement, the specific band alignment and strain effects. Therefore, influencing the structural properties, we are able to tune the electronic and optical properties (band gap engineering) of these materials. A 3D ordering of the QDs in regular lattices introduces additional possibilities in the material engineering due to collective effects which appear in periodic structures.

A recently published theoretical work about excitonic properties of Ge/Si and Si/Ge core/shell QDs [1] predicts type II of charge-carrier confinement in such structures and the appearance of a single dominant absorption peak with much larger oscillator strength than for peaks found in pure Si and Ge QDs. Additionally, a significantly different exciton lifetime and temperature dependencies are expected. Such materials are excellent for photovoltaic applications due to the absence of separation barriers for at least one type of carrier [2, 3, 4].

Intensive investigations have been performed on Si/Ge layer systems and self-assembled *epitaxial* Ge QDs produced in Si matrices [3, 5, 6, 17]. Ge/Si nanowires with core/shell structure are also extensively studied both theoretically and experimentally [7, 8, 9, 10, 11, 12].

However, in spite of the fact that there are several theoretical works proposing very attractive electronic properties of core-shell Ge/Si and Si/Ge QDs or nanoparticles [1, 13, 14], there are still practically no experimental reports on their preparation. Ge QDs on Si surface overgrown with Si layer were produced[15], and some indications of Ge/Si core/shell QDs were presented in Ref. [16], but without any systematic analysis and following works.

Here we report on the formation of small Ge/Si QDs showing a core/shell structure in an amorphous material, where the Ge core is slightly displaced from the center of the Si shell. The dots are spontaneously but regularly ordered in a body centered tetragonal (BCT) QD lattice inside an alumina glass matrix, and have a narrow size distribution. Such ordering is achieved by self-assembled growth during magnetron sputtering deposition of an Al_2O_3/Ge/Si multilayer film. The inversion of the Ge and Si deposition sequence results in the formation of two-dimensional Si/Ge structures in the form of very thin continuous layers instead of QDs. Therefore the wetting behavior of the Ge or Si atoms on the Al_2O_3 surface under the given growth conditions is the driving force for the formation of QD's. Furthermore, the growth conditions are chosen in such a way that almost no intermixing between Ge and Si atoms in these structures can occur. The as-grown QDs and layers are amorphous, while their crystallization is achieved by annealing at 800°C without affecting the sharp Ge/Si interfaces and a regular arrangement of the QDs.

The vibrational and optical properties of these materials are significantly different than those of the corresponding pure Al_2O_3/Ge, Al_2O_3/Si, and mixture Al_2O_3/GeSi systems, and they follow the theoretical predictions given in Ref. [1]. Namely, the Ge/Si material with core-shell QDs shows a single strong absorption peak, while a slightly broader but also single strong peak is found for the layered Al_2O_3/Si/Ge film. All other films show broad and/or low-intensity absorption bands. These properties support the specific band alignment and type II-confinement in the core-shell QDs,

in which the minimum of the valence band and the maximum of the conduction band are not in the same material.

The paper is organized as follows. In the first section of the paper we present the methods for the preparation and analysis of the investigated materials. Then we show the structure properties of the investigated systems including the shape and arrangement of the formed nanostructures as well as their crystalline structure. At the end, we present the results of the optical measurements.

2. Materials and methods

Five types of multilayer films were investigated: (i) Al_2O_3/Ge/Si ×30, (ii) Al_2O_3/Si/Ge ×30, (iii) Al_2O_3/Ge ×30, (iv) Al_2O_3/Si ×30, and (v) Al_2O_3/(Ge+Si)×30. All films were covered by one additional layer of Al_2O_3. The first two types are the samples of interest, while the last three are the reference samples. For simplicity of notation we omitt the Al_2O_3 part of the film composition in its name, so for example the film Al_2O_3/Ge/Si will be denoted as Ge/Si. The samples are produced by magnetron sputtering deposition at the KJLC CMS-1 magnetron system at 300°C on Si(111) substrates. The base pressure was in the range of $10^{-6} - 10^{-5}$ Pa, while the Ar pressure was 0.66 Pa in a continuous flow (13 ccm/min). The deposition conditions were chosen so that we deposited the same amounts of Ge and Si atoms within each period (the deposition times for Ge and Si were 45 and 132 s, using DC magnetrons operating at 10 and 54 W respectively). Al_2O_3 was deposited for 100 s using a RF power supply operated at 300 W. The Ge and Si reference samples were produced using the same deposition times and powers of Ge and Si as used for the Ge/Si films, while each Ge+Si layer in the mixed (Ge+Si) reference sample (denoted by GeSi in the following text) was deposited for 45 s, using powers 15 and 158 W for Ge and Si, respectively (adjusted to have the same amounts of Ge and Si atoms). The as-grown films were annealed in vacuum at temperatures up to 1000°C for 1 h.

Time-of-Flight Elastic Recoil Detection Analysis (TOF-ERDA) measurements were performed at the 6 MV tandem van de Graaff accelerator at the Rudjer Bošković Institute. For the measurements, 25 MeV $_{127}I^{6+}$ ions were used. High-resolution transmission electron microscopy (HRTEM) was carried out using a Titan 80-300 electron microscope (FEI) equipped with a field emission gun working at 300 kV and an image corrector to minimize the spherical aberration of the objective lens. Grazing incidence small angle x-ray scattering (GISAXS) was performed at the synchrotron Elettra, Trieste, using the photon energy of 8 keV, and a two-dimensional detector. The crystal structure of the samples was studied by x-ray diffraction (XRD) performed on a standard laboratory diffractometer using a CuKα radiation, parabolic multilayer optic and a parallel-plate collimator in front of a point detector. All the diffraction patterns were measured with the constant grazing incidence angle of 0.5 deg, i.e. close to the critical angle of total external reflection. An Ar ion laser with the excitation line of 514.5 nm and the DILOR Z-24 triple monochromator were used for the Raman measurements. Ellipsometric measurements were performed with a VASE Ellipsometer from J. A. Wollam Co., Inc. in the spectral range between 1 and 5 eV.

3. Results and discussion

We confirmed by ToF-ERDA that both types of samples (Ge/Si and Si/Ge multilayers) have

almost the same chemical compositions, i.e., the same atomic percentages of Ge, Si, Al, and O, namely, $c_{\rm Ge}^{\rm Ge/Si} = (8.6 \pm 0.6)\%$, $c_{\rm Si}^{\rm Ge/Si} = (8.6 \pm 0.9)\%$, $c_{\rm Al}^{\rm Ge/Si} = (31 \pm 1)\%$ and $c_{\rm O}^{\rm Ge/Si} = (50 \pm 3)\%$ for film Ge/Si and $c_{\rm Ge}^{\rm Si/Ge} = (8.2 \pm 0.9)\%$, $c_{\rm Si}^{\rm Si/Ge} = (10 \pm 1)\%$, $c_{\rm Al}^{\rm Si/Ge} = (30 \pm 2)\%$ and $c_{\rm O}^{\rm Si/Ge} = (50 \pm 3)\%$ for film Si/Ge. The traces of H and Ar are found in the films. The nearly same total amounts of Ge and Si atoms were found in the reference samples. The atomic composition of the films is found to be homogeneous through the whole film thickness. The chemical composition of the mixed GeSi layer was $\rm Ge_{0.45}Si_{0.55}$, what is close to the desired half-half Ge-Si ratio. The measured atomic composition will be compared to the number of atoms calculated from the models of the material structure in the following text.

The structures of the Ge/Si and Si/Ge multilayers are demonstrated in Fig. 1. For the first film, a formation of a regular array of ellipsoidal QDs is visible in the TEM image of the film (Fig. 1). The regularity in ordering is also nicely visible in the GISAXS map of this film (Fig. 1(b)), where sharp intensity maxima appear, caused by the correlation of the QD positions. The ordering in the QD lattice with an ABAB... stacking sequence, corresponding to a 3D BCT lattice, is strongly supported by the TEM results, and confirmed by the intensity distribution of the GISAXS image. The BCT lattice is defined in a Cartesian coordinate system with three nearest neighbor basis vectors $\mathbf{a}_1 = [a, 0, 0]$, $\mathbf{a}_2 = [0, a, 0]$ and $\mathbf{a}_3 = [a/2, a/2, c]$, where a is the QD in-layer separation and c is the multilayer period. The lateral distance between ordered QDs in the TEM image is found to be $a = (6.6 \pm 0.2)$ nm, the multilayer period $c = 4.0 \pm 0.1$ nm, while the lateral and vertical radii of the dots (R_L and R_V respectively) are found to be $R_L = (2.3 \pm 0.5)$ nm, and $R_V = (1.9 \pm 0.5)$ nm.

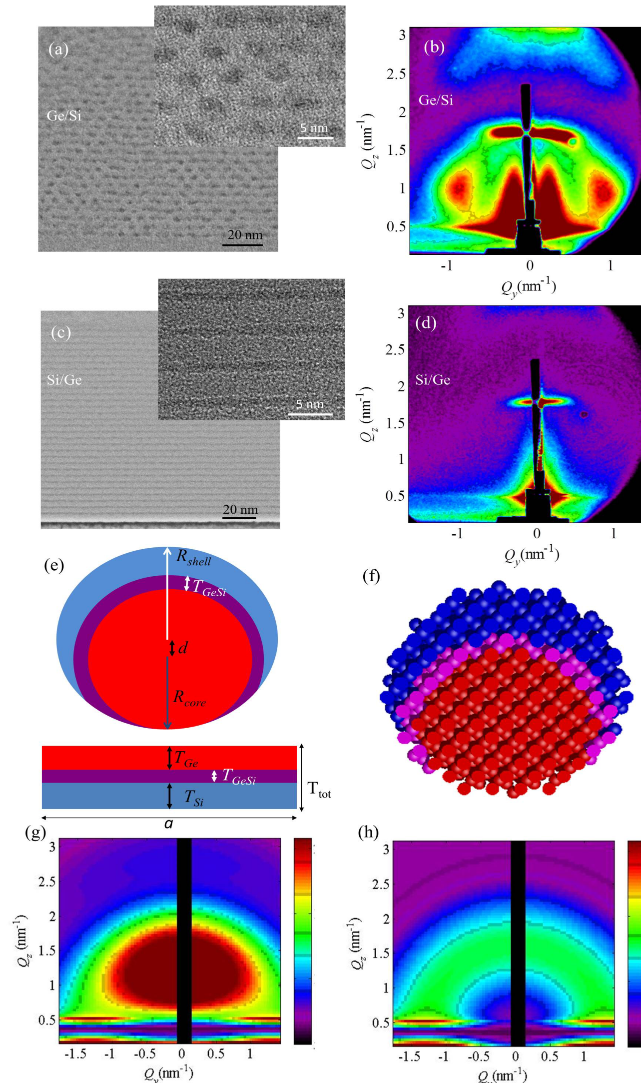

Figure 1. (Color online) Cross-section bright field TEM images (a,c) and corresponding GISAXS maps (b,d) of the as-grown Ge/Si (a,b) and Si/Ge (c,d) multilayers. The insets in panels (a) and (c) are showing the HRTEM images. (e) The models of the QD and layer structure used for the modeling of the experimental data: QD is assumed spherical with the core/shell structure, where the core is shifted from the center of shell by vector **d**; Layers are assumed to consist of three sub-layers consisting of Ge, Si and GeSi; a denotes the in-plane parameter of the BCT QD lattice. It is used to estimate the volume of the layer structure that corresponds to single QD. (f) Atomic model of the core/shell QD structure constructed using the parameters of the GISAXS fit. (g), (h) Form factors of the Ge/Si core/shell QD with shifted and non-shifted origins respectively. The parameters are taken from the fit.

The regular ordering is achieved in the whole volume of the film and remains stable during annealing up to 800°C. However, the ordering is destroyed in both types of the films during annealing at 900°C.

The structure of the multilayers deposited with the *inverted* order of Ge and Si under the same conditions is demonstrated in Figs. 1 (c,d). The structure of this film is completely different from the Ge/Si case, showing the formation of continuous layers instead of QDs. The same structure follows from the GISAXSs map of the film containing only the Bragg sheets caused by multilayer periodicity. The lateral intensity satellites (stemming from the lateral ordering of the QDs) like in Fig. 1(b) are not visible. The total thickness of the layers containing Ge and Si ($T_{\mathrm{tot}} = T_{\mathrm{Ge}} + T_{\mathrm{Si}} + T_{\mathrm{GeSi}}$, see Fig. 1(e)) is found to be 1.2 ± 0.8 nm, while the multilayer period c is the same as for the Ge/Si case (4.0 ± 0.1 nm).

The HRTEM images of the film cross-sections are shown in the insets of Figs.1(a,c). Although we can see nicely the internal structure of the dots, and find it amorphous, it is impossible to distinguish their Ge and Si parts. It is important to note that there are no remains of continuous Ge and/or Si layers visible in Ge/Si based film (like for the Si/Ge case), which strongly indicates that most of the Ge and Si atoms are incorporated indeed in the formed clusters, as will be shown later. The continuous layers are nicely visible in the Si/Ge based film.

In order to obtain details of the structural properties of the QDs in the Ge/Si multilayers, we have fitted the measured GISAXS maps to a theoretical formula based on the paracrystal model described in Ref. [21]. We have assumed that the QDs are arranged in a disordered BCT lattice with the average basis vectors $\mathbf{a}_1$, $\mathbf{a}_2$ and $\mathbf{a}_3$, defined in the text above. We found that standard form-factors of a single QD (spherical, ellipsoidal or centrosymmetric core-shell shapes) did not yield a good match, and the values of R_V determined from the fit were significantly smaller than from the TEM images. Therefore, we have used a modified form-factor of a core-shell QD, in which the core with the radius $R^{(\mathrm{core})}$ is shifted from the centrum of the shell ($R^{(\mathrm{shell})}$) toward the substrate by vector $\mathbf{d}$ (see Fig. 1(e)). The thickness of the mixed interface layer is denoted by T_{GeSi}. The electron densities were set to the literature values for Ge, Si and GeSi at the beginning of the fitting process. The form factors of the QD having the core/shell structure with the shifted origing (which was used in the fit) and the corresponding form factor obtained with no core shift are given in Figs. 1 (g) and (h) respectively. The numerical analysis of the GISAXS data from Ge QDs in Al_2O_3 matrix, always lead to the perfect agreement with the TEM data (please see Refs. [22]-[20]). Additionally, the GISAXS measurements provide the structural information with excellent statistics. Therefore we believe it is that the numerical analysis of the GISAXS data combined with the TEM is excellent proof for the core/shell structure of the very small QDs, for which other methods cannot be applied.

As we have BCT ordering of the QDs, and the same amounts of atoms in both films, the area of the Si/Ge bilayer that corresponds to a single Ge/Si QD is a^2. All parts of the QD are assumed to be elongated in the direction parallel to the surface by a factor f, so $\mathrm{R}_L^{(\mathrm{core,shell})} = fR^{(\mathrm{core,shell})}$, and $R_V^{(\mathrm{core,shell})} = R^{(\mathrm{core,shell})}$. The best fit was obtained for $R_V^{(\mathrm{core})} = (1.59 \pm 0.05)$ nm, $R_L^{(\mathrm{core})} = (1.75 \pm 0.05)$ nm, $R_V^{(\mathrm{shell})} = (2.04 \pm 0.05)$ nm, and $R_L^{(\mathrm{shell})} = (2.35 \pm 0.05)$ nm, while the thickness of the interface layer T_{GeSi} is found to be (0.31 ± 0.05) nm and the shift of the origin

$d = (0.71 \pm 0.05)$ nm what is very slightly larger than $R_V^{(shell)} - R_V^{(core)}$. The obtained size of the QDs (shell size) agrees excellently with the TEM values. The size dispersion is quite low (standard deviation is 0.35 nm), showing the formation of size-uniform clusters. The electron densities were only slightly modified with respect to the initial (nominal) values.

The parameters a and c of the QD lattice are found to be: $a = (6.7 \pm 0.1)$ nm, and $c = (3.95 \pm 0.05)$ nm. From these parameters and from the QD radii we calculated the total volumes of the core and shell parts of the QDs in unit volume of the multilayer, and from these volumes we estimated the atomic concentrations of Ge and Si (assuming that QDs consist of pure Ge and Si). The obtained concentrations ($c^{Ge/Si}_{Ge,GISAXS} = (9 \pm 1)\%$ and $c^{Ge/Si}_{Si,GISAXS} = (9 \pm 1)\%$ are in excellent agreement with the concentrations found by the TOF-ERDA measurements, showing that all Ge and Si atoms are indeed incorporated in the QDs. This agreement also supports the core/shell structure of the dots.

The structure of the reference samples (pure Ge, Si and Ge+Si films) is demonstrated in Fig. 2. The formation of the Ge QDs arranged in a BCT QD lattice was achieved as expected for the Ge film [20], while Si layers and Ge+Si mixed layers form continuous layers over alumina instead of QDs. Using these facts we can easily understand the structure of the above presented Ge/Si- and Si/Ge-containing multilayers. From our previous work (please see Ref. [20]) we know that Ge QDs form after the deposition of the Al_2O_3/Ge sequence. So, the addition of the Si layer on the formed Ge QDs causes covering of them by Si. Thus, taking into account the GISAXS measurements there are three possibilities for the material structure: (i) Si covers the Ge QDs as a continuous layer, (ii) Si preferentially cover Ge QDs but it is mixed with Ge and form GeSi QDs, and (iii) Si preferentially cover Ge QDs forming the core/shell structure without significant mixing. From the TEM measurements it is clear that Si does not make the continuous layer over Ge QDs. From the number of Ge and Si atoms it clearly follows that the QDs consist of both Ge and Si; if they would consist of only Ge they will be significantly smaller. Thus the first option is in contradiction with our measurements. The second (ii) case is not likely to happen due to the low deposition temperature at which the interdiffusion of Si and Ge is very low. So, the Si is placed around formed Ge QDs and the core/shell structure is the most likely to happen. Finally, the anisotropic core/shell structure is formed due to the fact that Ge QDs are formed first in the deposition sequence, and that they are attached to the Al_2O_3 layer below it. It is logical that Si covers them more on their top side, so the anisotropic core/shell structure is formed. For the Si/Ge deposition sequence, the formation of a continuous Si layer again on the Al_2O_3, prevents the formation of Ge clusters, so the Ge atoms are deposited on the Si layer underneath without creating the dots.

The Ge is stable for annealing up to 700°C; the disintegration of the film and a detectable Ge-loss appears only at 800°C. Si remains stable up to 1000°C, with no clustering observed, while the clustering starts at 600°C for the mixed Ge+Si film. However there is no material loss during annealing up to 1000°C for the mixed film.

The crystalline structure of the measured films is demonstrated in Fig. 3, where we plot x-ray diffraction curves. From the figure it is evident that the films annealed up to 700°C are mainly amorphous, while both films annealed

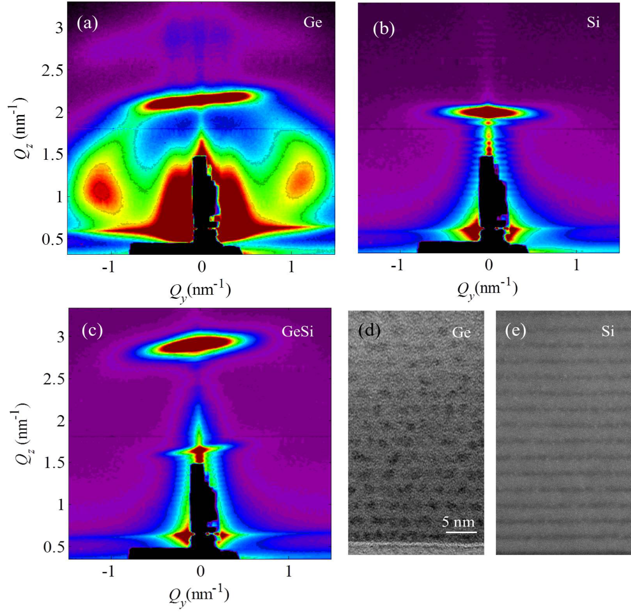

Figure 2. (Color online) GISAXS maps of the as-grown (a) Ge, (b) mixed GeSi and (c) Si films. (d) TEM images of the pure Ge and Si films.

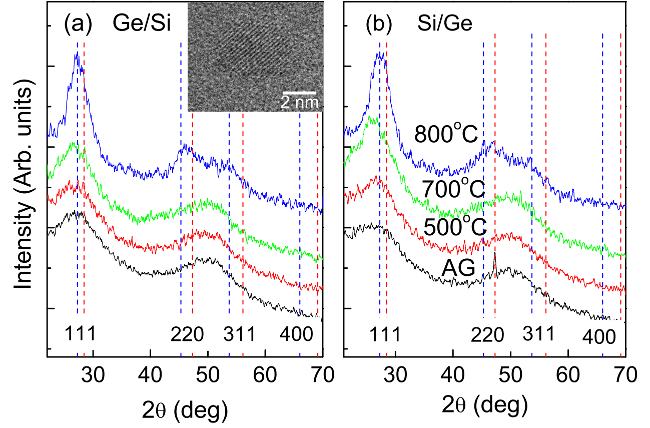

Figure 3. (Color online) X-ray diffraction curves of the (a) Ge/Si, (b) Si/Ge films. The annealing temperatures are indicated in panel (b). The positions of crystalline peaks for Ge and Si are denoted by blue and red vertical dotted lines respectively, along with the diffraction indexes. Inset: crystallized QD just at the threshold of crystallization (700C) the 220 net planes are visible.

at 800°C are crystalline. The crystallization is estimated to start at 700°C, as the peaks for this annealing temperature are slightly narrower than for the lower temperatures. This is supported by HRTEM analysis which shows the crystallization of some QDs (inset of Fig. 4). For the annealing at 800°C, three Ge-related crystalline peaks can be distinguished: (111), (220) and (311). The peaks are relatively broad for both film types due to the very small sizes of the formed nanocrystals and coexistence of Ge and Si, therefore, it is impossible to draw any reliable conclusion about the core/shell structure from the XRD measurements. The pure Ge-based sample showed the crystallization at 700°C, while only broad peaks were visible for the Si based film for all temperatures up to 800°C.

Raman spectroscopy is sensitive to the vibrational modes of Ge-Ge, Ge-Si and Si-Si bonds, so we apply it for the additional structure analysis. The Raman spectra measured on Ge/Si and Si/Ge based films, as grown and annealed at different temperatures are shown in Figs. 4 (a) and (b) respectively. All spectra show bands typical for Ge-Ge, Ge-Si and Si-Si vibrations [19]. All bands are broad, what is the characteristic of amorphous material or very small crystalline structures. All spectra look similar for the same type of the film, even for the higher annealing temperatures. The relative intensities of these bands (deduced from the peak areas after deconvolution) differ for Ge/Si- and Si/Ge-based films, and the Si-Ge band at 380 cm^{-1} is 1.45 times stronger for the Si/Ge film than for the film with Ge/Si QDs. This fact indicates that the Si/Ge-based film has more Ge-Si bonds than the Ge/Si films with QDs.

In order to have a complete insight in the structural changes of the films during annealing and to be able to separate the contributions from the Ge, Si and GeSi parts

of the film, we consider also the Raman spectra from the pure Ge, Si and GeSi mixture based films (Fig. 4 (c)-(e)). The pure Ge films show the typical amorphous structure of an as-grown film, while the film annealed at 700°C exhibits only the *c*-Ge (crystalline-Ge) contribution. The film annealed at 800°C has no Ge-related bands, which indicates a disintegration of the film, and a Ge loss. This is in accordance with the GISAXS results and the previous investigations of Ge films [22]. The GeSi mixture film (Fig. 4(d)) has the strongest Si-Ge band and the spectra are similar for all annealing temperatures. The Si-based films show very weak amorphous Si-related bands for the as-grown film (Fig. 4(e)). The Si signal from the nanostructures was impossible to separate from the contribution of the Si substrate for the higher annealing temperatures, where crystalline nanoparticles were expected.

For the quantitative analysis and determination of the individual layer thicknesses in the Si/Ge film we have used the standard procedure for fitting the Raman spectra of Si/Ge layers described in Ref. [17] and the references therein. The total Raman intensity is a superposition of the Raman contributions from the Ge, Si and mixed GeSi layers weighted by their absorption factor (α) and "spectroscopic" layer thickness (t) which is proportional to the real thickness (T): $I = t_{\mathrm{Ge}}\alpha_{\mathrm{Ge}}I_{\mathrm{Ge}} + t_{\mathrm{Si}}\alpha_{\mathrm{Si}}I_{\mathrm{Si}} + t_{\mathrm{GeSi}}\alpha_{\mathrm{GeSi}}I_{GeSi}$. Absorption in alumina matrix is neglected due to the significantly smaller absorption coefficient. The absorption factors for the wavelength of laser used for the Raman measurements, (514.5 nm) were measured for each film and presented in Fig. 5. The real layer thicknesses are obtained by normalizing of the spectroscopic thicknesses (t) to the measured thickness T_{tot} (see Fig. 1(e)) of the layer containing

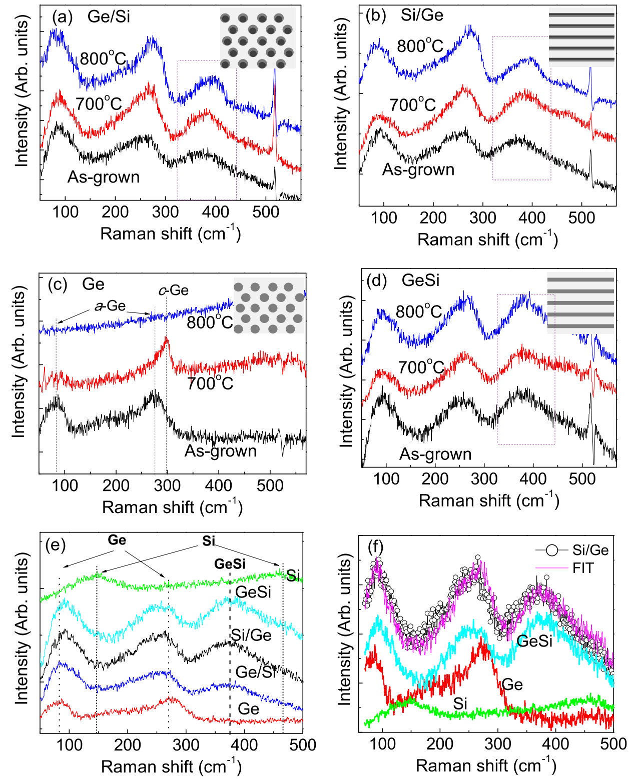

Figure 4. (Color online) (a), (b) Raman spectra of the as-grown and annealed Ge/Si and Si/Ge films respectively. The temperatures are indicated in the figure. (c),(d) Spectra of the Ge and GeSi films. (e) Comparison of all spectra including Si for the as-grown films. The positions of Ge-Ge, Si-Ge and Si-Si vibrational bands are indicated in the figure. (f) Result of the fitting procedure of the spectra measured on Si/Ge film described in the text.

Ge and Si: $T_{\mathrm{Ge}} = t_{\mathrm{Ge}}T_{\mathrm{tot}}/(t_{\mathrm{Ge}}+t_{\mathrm{Si}}+t_{\mathrm{GeSi}})$. The value of T_{tot} was determined from the HRTEM measurements.

The result of the fitting of the Raman spectra for the Si/Ge based film, as well as the individual contributions (pure Ge, Si, and GeSi based films) are given in Fig. 4(f). The Ge, Si and their interface GeSi layer thicknesses obtained from the fit are: $T_{\mathrm{Ge}} = (0.50 \pm 0.03)$ nm, $T_{\mathrm{Si}} = (0.54 \pm 0.03)$ nm and $T_{\mathrm{GeSi}} = (0.18 \pm 0.05)$ nm.

Using these thicknesses, and the value of the multilayer period for Si/Ge-based film,

we have calculated the atomic percentages of Ge and Si atoms within the layers (assuming that the layers are made of pure Ge and Si) and compared them with the ToF-ERDA measurements. The obtained concentrations ($c^{\rm Si/Ge}_{\rm Ge,Raman} = (8.8 \pm 0.8)\%$ and $c^{\rm Si/Ge}_{\rm Si,Raman} = (10 \pm 1)\%$ are again in the excellent agreement with the ToF-ERDA results, while the thickness of the mixed layer is similar to the one obtained for Ge/Si case by GISAXS.

We were not able to fit the spectra of the annealed films, since the strong phonon confinement influences significantly the shape and positions of the crystalline peaks. In particular, the evaluation of the Ge contribution is problematic because Ge is located only in the QDs, which results in a very strong confinement. While the amorphous Ge-related bands are broad and not significantly influenced by the QD-size effect, the Ge crystalline peak is relatively narrow and strongly affected by the QD size [23]. However, the very similar shape of all Raman spectra of the same film type means that the ratio of the Si, Ge and GeSi contributions is nearly the same for all annealing temperatures which indicates the same Ge, Si and GeSi layer thicknesses in all films.

The interface layer thicknesses $T_{\rm GeSi}$ for Ge/Si and Si/Ge films determined from the fitting of the Raman spectra in this work (see above) are significantly smaller than the interface layer thickness obtained for Si/Ge films prepared in a glow discharge reactor (0.7 ± 0.2) nm, reported in Ref. [19] or by plasma enhanced chemical vapor deposition (PECVD) [18], where a thickness of (0.5 ± 0.1) nm was found. The mean value of the interface thickness obtained here (0.25 ± 0.05) nm is very similar to the value obtained for Si/Ge layers prepared by also by PECVD but using the plasma interruption after completing each layer (0.24 ± 0.02) nm[17], which is similar to the procedure that we have used.

Additional confirmation of the thickness value of the Ge/Si interface layer comes from the comparison of the intensity of the Si-Ge peak for Ge/Si and Si/Ge based films. As we stated above, the intensity of the Si-Ge band (see Fig. 4) is 1.45 times larger for the Si/Ge than for the Ge/Si -based film. This shows a different number of Si-Ge bonds in these films, since the numbers of Ge and Si atoms in both films are the same. We believe that the difference of the number of the bonds is caused by a different Ge/Si interface area in the Ge/Si QDs and Si/Ge layered films. Therefore, we compare the volumes of the interface layers in the Ge/Si QD and the corresponding part of Si/Ge layer (see the schemes given in Fig. 1 (f)). Assuming the same thickness of the interface layer of (0.25 ± 0.05) nm, the result of the comparison gives the volume ratio of $V^{\rm (mixed)}_{\rm Si/Ge}/V^{\rm (mixed)}_{\rm Ge/Si} = 1.45 \pm 0.09$, which is in excellent agreement with the ratio of the areas of the Raman GeSi peaks for these two films. Thus, the analysis of the intensity GeSi Raman band at 480 $\rm cm^{-1}$ also strongly supports the formation of Si/Ge layers and Ge/Si core/shell nanoparticles with the sharp interface between Ge and Si parts.

Finally, in Fig. 5 we present the optical properties of the films. For the data analysis, the composite Ge/Si films were represented as single homogeneous layers, the effective optical constants of which were modeled by a flexible multiple-oscillator model [24]. The imaginary part of the effective dielectric function ϵ_2 and the corresponding absorption coefficients are presented for the as-grown and 800^oC annealed films. Since the Al_2O_3 matrix is transparent in the considered spectral range, all absorption effects can be ascribed solely to the presence

of Si and Ge.

The absorption bands of pure Si and Ge films, shown in Fig. 5, are broad and increasing towards higher energies. In the case of Ge, ϵ_2 has broad bands centered around 2.2 and 4.5 eV that can be associated to the E_1 and E_2 critical points of the band structure; the bands are broadened and blue-shifted with respect to the bulk material values due to quantum confinement effects [25]. Upon annealing at 800°C, these bands disappear due to the disintegration and a consequent decrease in the absorption of the Ge films [24]. Similarly, the broad bands observed for Si films at 3.2 and 4.5 eV can be connected to E_1 and E_2 critical points of crystalline Si broadened due to confinement effects [26].

The Ge/Si and Si/Ge based films have significantly different absorption properties. The absorption is much stronger, than for the case of the pure films, the peaks are narrower, better pronounced and they appear at different energies. The as-grown Ge/Si film shows a strong peak at 2.8 eV, which becomes better pronounced for the annealed film. The absorption in the as-grown Si/Ge film also shows a single but broader peak at 2.6 eV, which narrows down during annealing. The absorption in the mixed films is also quite strong, but the peaks are significantly broader.

Overall, the observed behavior is in the excellent agreement with the theoretical predictions from Ref. [1] where the absorption properties for Ge/Si and Si/Ge quantum dots with core-shell structure are calculated. The good agreement with the theory supports strongly the formation of Ge/Si core/shell structure with sharp interface between Ge and Si. Strictly speaking the comparison can be done only with the Ge and Ge/Si QDs, because in all other films layers are present instead of QDs. The absorption of Ge is broader and

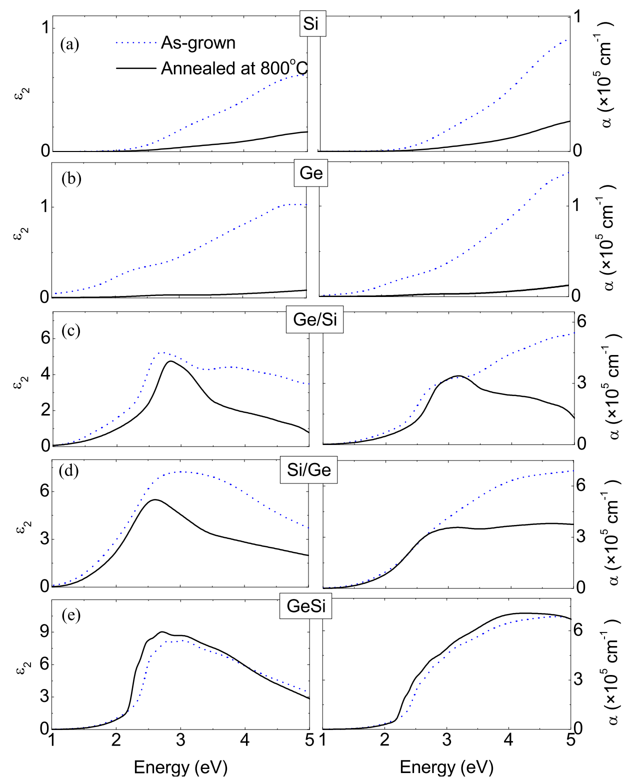

Figure 5. (Color online) Imaginary part of the dielectric function for the as-grown film and annealed films at 800°C: (a) Si (b) Ge, (c) Ge/Si, (d) Si/Ge and (e) GeSi films.

blue-shifted compared to the Ge/Si.

The lowest-energy Ge peak from Ref. [1] appear at lower energy with respect to the Si peak. The same is observed here, but the peak positions for both Ge and Si are shifted toward lower energies because we have slightly larger QDs (weaker confinement effects) than the values used for the theoretical predictions.

The Ge-related bands appear at lower energies than both Ge/Si and Si/Ge based films what is also in excellent agreement with the prections. Most important, the difference of the absolute values of the absorption coefficients can be connected to the much larger dipole transition moments that take place on the Ge/Si system compared to Ge or Si QDs.

Interestingly, the Si/Ge system shows a

peak that is red-shifted with respect to the Ge/Si peak, in agreement with the theoretical prediction for core-shell, that suggests that a similar absorption mechanism dominates the Si/Ge samples although no core-shells are formed. It has to be mentioned that these results are supported by direct calculation of optical losses from reflectance and transmittance on films deposited on quartz substrates, that revealed the presence of a characteristic peak at 2.8 eV for the Ge/Si system.

4. Summary

We have produced three-dimensionally ordered Ge/Si quantum dots with core/shell internal structure in alumina glass matrix by a simple magnetron sputtering deposition process of Al_2O_3/Ge/Si multilayer film. The inverted deposition sequence resulted in a completely different structure consisting of thin continuous Si/Ge layers within the alumina matrix, due to different wetting behavior of the Si/Ge on Al_2O_3. Both produced structures have a very sharp interface between the Ge and Si parts of the dots and layers. The materials show strong effects of confinement, band alignment and strain effects and have significantly different light absorption properties than pure Al_2O_3/Ge and Al_2O_3/Si films. According to the theoretical predictions, the presented materials are very suitable for applications in photovoltaics.

Acknowledgements

The authors are grateful to Aleksa Pavlešin for the help in the sample preparation. MB, NR, MJ, TC acknowledge Adris Group for the donation and Croatian Science Foundation (pr. no. 234) which supported this investigation.

References

[1] Oliveira E L, Albuqerque E L, de Sousa J S, Farias G A and Peeters F M (2012) *J. Phys. Chem. C* **116** 4399
[2] Shik A, Ruda H and Sargent E H 2001 *Nanotechnology* **12** 523
[3] Grützmacher D, *et al.* 2007 *Nano Lett* **7** 3150
[4] Kim S, Fisher B, Eisler H J and Bawendi M 2003 *J. Am. Chem. Soc.* **125** 11466
[5] Le Thanh V 2001 *Surf. Sci.* **492** 255
[6] Stangl J, Holy V and Bauer G 2004 *Rev. Mod. Phys.* **76** 725
[7] Xiang J, Lu W, Hu Y, Lieber C M 2006 *Nature* **441** (2006) 489
[8] Qian F, Li Y, Gradecak S, Park H G, Dong Y, Ding Y, Wang Z L and Lieber C M 2008 *Nature Mater.* **7** 701
[9] Peng X, Logan P 2010 *Appl. Phys. Lett.* **96** 143119
[10] Lauhon L J, Gudiksen M S, Wang D and Lieber C M 2002 *Nature* **420** 57
[11] Kempa T J, Day R W, Kim S K, Park H G and Lieber C M 2013 *Energy Environ. Sci.* **6** 719
[12] Nguyen B M, Taur Y, Picraux S T and Dayeh S A 2014 *Nano Letters* **14**(2) 585
[13] Asaduzzaman A M and Springborg M 2006 *Phys. Rev. B* **74** 165406
[14] Ramos L E, Furthmuller J and Bechstedt J 2005 *Phys. Rev. B* **72** 045351
[15] Ogawa Y, Toizumi T, Minami F and Baranov A V 2011 *Phys. Rev. B* **83** 081302
[16] Yang C S and Kauzlarich S M 1999 *Chem. Mater.* **11** 3666
[17] Sette F, Abeles B, Yang L, Mac Dowell A A, Richardson C H and Norman D 1988 *Phys. Rev. B* **37** 2749
[18] Persans P D, Rupert A F, Abeles B and Tiedje T 1985 *Phys. Rev. B* **32** 5558
[19] Santos P V and Ley L 1987 *Phys. Rev. B* **36** 3325
[20] Buljan M, Radić N, Ivanda M, Bogdanović-Radović I, Karlušić M, Dražić G, Pletikapić G, Svetličić V, Bernstorff S and Holy V 2013 *J. Nanopart. Res.* **15** 1485
[21] Buljan M, Radić N, Bernstorff S, Dražić G, Bogdanović-Radović I and Holy V 2012 *Acta Crystallogr. A* **86** 124
[22] Buljan M, Jercinovic M, Siketic Z, Bogdanovic-Radovic I, Delac Marion I, Kralj M, Ivanda M, Turkovic A, Drazic G, Bernstorff S and Radic N 2013 *J. Appl. Cryst.* **46** 1490
[23] Campbell I H and Fauchet P M 1986 *Sol. State.*

Comm. **58** 739

[24] Janicki V, Sancho-Parramon J, Zorc H, Salamon K, Buljan M, Radić N and Desnica U 2011 *Thin Solid Films* **519** 5419

[25] Alonso M I, Garriga M, Bernardi A, Goni A R, Lopeandia A F, Garcia G, Rodriguez-Viejo J and Labar J L 2008 *Thin Solid Films* **516** 4277

[26] Price J and Diebold A C 2006 *J. Vac. Sci.* **24** 2156